Demonstration of CTE-Matched Two-Phase Minichannel Heat Sink

Mohammad Reza Shaeri, Chien-Hua Chen, Richard W. Bonner, Maksym Demydovych
Advanced Cooling Technologies, Inc., Lancaster, PA, 17601, USA
MohammadReza.Shaeri@1-ACT.com

***Abstract*—Pumped two-phase cooling systems have been identified as effective thermal management solutions to remove a large amount of heat, provide excellent temperature uniformity across the device, and operate within low pumping power compared to their single-phase liquid-cooled counterparts. Regardless of the mechanism of heat transfer, effective materials for an efficient thermal management are those with high thermal conductivity to enhance the heat dissipation, and low coefficients of thermal expansion (CTE) to minimize thermal stress. In addition, the CTEs of the materials adjacent to each other must be close to each other to avoid a CTE mismatch, which is a main reason for the device failure. In this study, a low-CTE two-phase minichannel heat sink was fabricated and tested in moderately high heat fluxes. The evaporator was a double bonded copper (DBC) aluminum nitride (AlN), which was brazed into a Kovar enclosure. Both AlN and Kovar are CTE-matched. Also, the heat sink was a dielectric cooling system due to a low dielectric constant of AlN and using the refrigerant R245fa as the working fluid. The AlN substrate allows a direct mounting the electronic on the substrate without using a thermal interface material. The experiments were conducted at two flow rates with high inlet subcooling degrees. The heat sink operated above 183 W/cm^2 without any indication of partial dryout. At this heat flux, the measured thermal resistances for both flow rates culminated in values ~ 0.32 K-cm^2/W.**

Keywords—Thermal management; Two-phase heat transfer; Minichannel heat sink; CTE-matched heat sink.

I. INTRODUCTION

As a key part of an electronic packaging, thermal management stands for providing a reliable operation for an electronic device. The rapidly ongoing trend of increasing the power of electronic components along with shrinkage in their size have made severe challenges for the thermal management of next generation of high heat density electronics [1]. Dissipation of highly concentrated heat using traditional air-cooled systems and pumped single-phase liquid cooling technologies lead to substantial shortcomings due to poor thermal properties of the air and requirement of a large pumping power, respectively [2]. However, such limitations can be potentially addressed using pumped two-phase systems like micro/minichannel heat sinks. These compact thermal management solutions (TMSs) offer dissipating a significantly larger amount of heat with improved surface temperature uniformity compared to their single-phase liquid-cooled counterparts at a given pumping power. Such advantages are due to leveraging the coolant's latent heat of vaporization, which is orders of magnitude larger than the specific heat capacity of most working fluids [3,4].

An efficient TMS should dissipate large amounts of heat from the electronic device, maintain the device temperature below a design limit, and minimize the temperature deviation across the device [5]. In case the TMS is an active cooling system, operation of the system with the minimum pumping power is another main requirement of an effective TMS. However, in addition to the aforementioned criteria, there are certain crucial factors such as long-life reliable operation of an electronic device that should be satisfied by selecting appropriate thermal packaging materials.

An effective electronic packaging material should have a high thermal conductivity and a low coefficient of thermal expansion (CTE) [6,7]. A high thermal conductivity enables dissipation of a large amount of heat from the heat source (e.g., chip). A low CTE reduces thermal stress across the cooling system and minimizes the risk of device failure. Generally, the CTE of heat spreader materials used in an electronics packaging should be in the range of 4-7 ppm/K to match the CTE of electronic components and packaging materials [8,9]. Although copper and aluminum are the most conventional high thermal conductivity materials for fabrication of heat sinks, their CTEs are large; therefore, a thermal interface material (TIM) is used to attach the electronics to the heat sink. However, adding a TIM that typically has a low thermal conductivity, results in an additional thermal resistance, which deteriorates the cooling performance. In addition, it is crucial that thermal packaging materials are CTE-matched with each other and with the electronic components to minimize thermal stress resulting from CTE-mismatch between them at their joints [9–11]. The thermal stress due to the CTE-mismatch between the electronic chips and the metalized substrates during thermal cycling has been identified as a primary failure in electronic power modules [12,13]. Using CTE-matched materials allows direct solder of the electronic components to the metalized substrate and elimination for using a TIM between the chip and the substrate, which substantially lower the overall thermal resistance between the chip and the coolant. As a result, direct solder of electronics

on the heat sink allows the electronics to operate in higher power and within safe operation temperatures.

In the present study, a two-phase minichannel heat sink with a substrate made of an aluminum nitride (AlN) ceramic with direct bonded copper (DBC) layers is fabricated and its thermal performance is demonstrated under various heat fluxes. AlN is a ceramic with an excellent thermal conductivity of ~ 150-200 W/m.K, high temperature stability, and a low CTE of ~ 4.5 ppm/°C [14]. The thin copper layer on both side of the AlN substrate enables sealing the Kovar envelope via direct metallurgical bonding, as well as soldering the electronics to the heat sink. Compared to using a TIM, a metallurgical bonding is substantially superior that leads to reduced thermal resistance. Besides, the copper layer on the AlN substrate allows sintered copper wick to further enhance thermal performance of the heat sink. Moreover, AlN has a low dielectric constant and has been demonstrated as an excellent alternative of printed circuit board (PCB). Compared with PCBs that usually suffer from poor thermal conductivity, DBC ceramic substrates have exhibited four times lower thermal resistance, and significant mitigation in the parasitic inductances [15]. These characteristics of AlN make AlN-Kovar two-phase minichannel heat sinks as excellent CTE-matched TMSs in high heat flux electronic/power applications.

II. Experiment

A. Two-Phase Cooling Loop

Fig. 1 illustrates the schematic of the cooling loop. The primary components of the loop consist of a heat sink, a positive displacement pump, a filter, pressure transducers, T-type thermocouples, a flowmeter, a control valve, a reservoir, a condenser, and a chiller. The components of the loop were connected to each other by stainless steel tubes. The pump circulated the refrigerant R245fa in the loop. The flow rate was adjusted and measured by the upstream control valve and the flowmeter, respectively. The inlet and outlet temperatures and pressures of the flow were measured by T-type thermocouples and pressure transducers, respectively, inserted at the inlet and exit of the heat sink. The outlet two-phase mixture was returned to the reservoir. To avoid the cavitation at the pump and ensure that the inlet liquid to the pump was liquid, the reservoir was connected to a heat exchanger that was acting as a condenser. The heat rejected from the two-phase mixture in the condenser was exchanged with a lower-temperature coolant (water) provided by the chiller.

The CAD model of the heat sink is illustrated in Fig. 2. The geometrical information of the heat sink is listed in Table 1. The heat sink encompassed one channel with a length (L), width (W), and height (H) of 11.1 mm, 8.6 mm, and 2.0 mm, respectively, which corresponded to a hydraulic diameter (D_h) of 3.2 mm:

$$D_h = 2\frac{W \times H}{W + H} \tag{1}$$

Kandlikar and Balasubramanian [16] categorized flow passages with $200\ \mu\text{m} \leq D_h < 3\ \text{mm}$ as minichannels, and those with $D_h \geq 3\ \text{mm}$ as conventional channels. Since the hydraulic diameter of the heat sink in the present study is close to that of the upper bond of a minichannel based on the categories in [16], the heat sink in this study is simply considered as a minichannel.

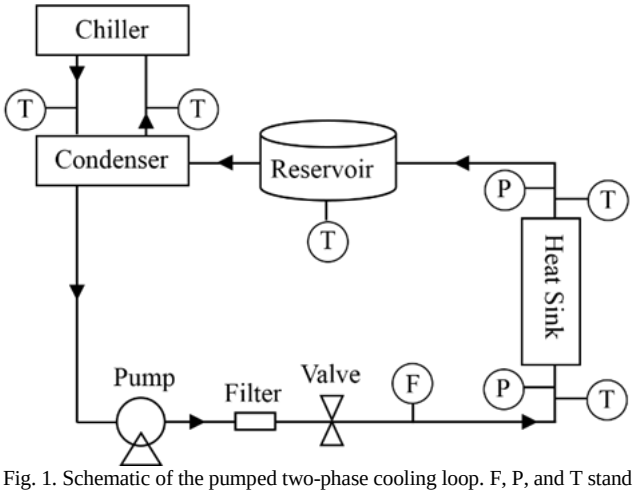

Fig. 1. Schematic of the pumped two-phase cooling loop. F, P, and T stand for flowmeter, pressure transducer, and thermocouple, respectively

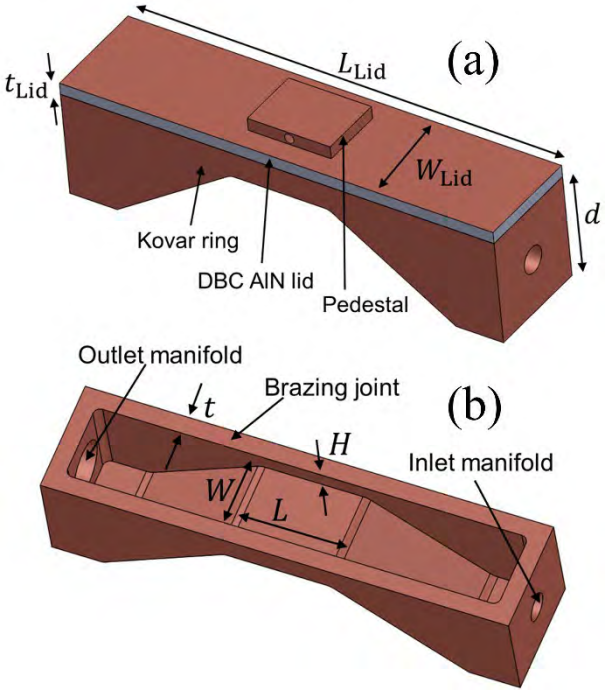

Fig. 2. CAD model of the heat sink. (a) Enclosure; (b) Exploded view.

The heat sink consists of a DBC AlN substrate, a copper plated Kovar support (ring), and a pedestal. The substrate had a thickness of 1.42 mm, which the thickness of AlN was ~ 1.02 mm, and two thin copper layers with a thickness of 0.20 mm were bounded on two sides of the AlN plate. The enclosure was made by brazing the AlN substrate on the copper plated Kovar support with a low CTE ~ 5.9 ppm/°C [17], which is CTE-matched with AlN. Brazing the DBC AlN substrate to the Kovar support allows for a hermetically sealed enclosure. The peak internal pressure inside the heat sink is dictated by the refrigerant

type as well as the operating conditions. Maintaining hermeticity of the heat sink, specifically in the peak internal pressure inside the heat sink, is crucial for a reliable operation of the heat sink. To lower the internal pressure of the heat sink, refrigerant R245fa was selected because of its reasonably low vapor pressure at common electronics operating temperature range. Also, one of the main parameters to maintain such hermeticity is the sufficient thickness of the brazing joint on the Kovar enclosure. During several fabrication tests, it was found that the optimal Kovar wall thickness for brazing to AlN plate while using R245fa as the working fluid should not be less than 2.0 mm; therefore, this value was used in the present experiment.

A pedestal, which was the location of placing the heater, was soldered on the substrate. A hole extended to the middle of the pedestal was created inside the pedestal. A T-type thermocouple was inserted inside the hole to represent the temperature of the heat source, as the highest temperature in the system. The space between the thermocouple and the hole was filled with a thermal grease. The electrical heat load was applied by a resistive heater soldered on the pedestal. The input heat was adjusted by regulating the voltage of a variable transformer that powered the resistive heater. Copper tubes were brazed into the inlet and outlet manifolds of the heat sink. The hermeticity of the heat sink was checked by a helium mass spectrometer with a measured leak rate less than 9×10^{-10} Std. cc/s. Prior to charging the loop with the refrigerant, the entire system was checked for possible leaks.

TABLE 1. Geometrical information of the heat sink.

Pedestal footprint area (A_S)	0.77 cm^2
DBC AlN plate thickness (t_{Lid})	1.42 mm: 1.02 mm AlN, and 0.2 mm copper layer at each side
DBC AlN plate length (L_{Lid})	53.1 mm
DBC AlN plate width (W_{Lid})	12.6 mm
Height of Kovar support (d)	12.7 mm
Channel length (L)	11.1 mm
Channel width (W)	8.6 mm
Channel height (H)	2 mm
Brazing joint thickness (t)	2 mm
Inlet manifold diameter	3.2 mm
Outlet manifold diameter	6.4 mm

The test started by circulating the liquid refrigerant throughout the loop and adjusting the pump speed to feed the heat sink at different flow rates. The experiments were performed at two flow rates of 0.31 and 0.51 LPM (liter per minute). Because dryout is accelerated at low inlet subcoolings [18], the present experiments were conducted at high inlet subcoolings. The degree of subcooling is calculated as $T_{sat} - T$, where T is the fluid temperature and T_{sat} is its corresponding saturation temperature at the liquid pressure. The corresponding inlet subcooling degree at the flow rates of 0.31 LPM and 0.51 LPM was ~ 12 °C and ~ 20 °C, respectively. By adjusting the temperature of the chiller, the inlet temperature was maintained in a narrow range of 10.2-10.4°C. The heat input to the heater was increased by regulating the voltage of the variable transformer. At each heat input, the data was collected when the system reached a steady state condition, which is determined by the changes of temperatures below 0.5 °C over a 15-min period of operation. Signals from the thermocouples, pressure transducers, flowmeter, and heater were collected using a Keithley 2700 data acquisition system. Fig. 3 illustrates the fabricated heat sink.

Fig. 3. Fabricated heat sink in the present study.

B. *Data Reduction and Uncertainty Analysis*

The heat sink was covered with a layer of insulation to minimize the heat loss to the environment. For calculating the heat loss, a widely accepted approach in the literature was used that represents the ratio of the effective heat absorbed by the working fluid (Q_{eff}) to the electrical heat input (Q_E) [19]:

$$\phi = \frac{Q_{eff}}{Q_E} \tag{2}$$

where ϕ is the heat transfer ratio. Calculation of heat loss in a two-phase cooling process is challenging since it requires to calculate the vapor quality inside the heat sink. To overcome this challenge, the heat loss in the present work was obtained through a series of single-phase cooling tests prior to the boiling and calculating a range of heat transfer ratios, as follows:

$$\phi = \frac{\rho \dot{V} c_p (T_{out} - T_{in})}{V \times I} \tag{3}$$

where V and I are the voltage and current applied to the resistive heater, respectively. ρ, $\dot{V}$, and c_p are the liquid density, volume flow rate, and specific heat, respectively. T_{in} and T_{out} are the fluid temperature at the inlet and outlet of the heat sink, respectively. Then, the mean value of $\phi = 0.89$ was used to calculate the effective heat flux, as follows:

$$q = \phi \frac{Q_E}{A_S} \tag{4}$$

where q represents the heat flux, and A_S is the footprint area of the pedestal, described in Table 1. In the preset study, thermal performance of the heat sink is described by thermal resistance (R), defined as follows:

$$R = \frac{T_S - T_{ref}}{q} \tag{5}$$

where T_S is the source temperature, and T_{ref} corresponds to the reference temperature calculated as the average of inlet and outlet temperatures:

$$T_{ref} = \frac{T_{in} + T_{out}}{2} \tag{6}$$

The uncertainties of the components used in the experiments were based on the information provided by their manufacturers.

The uncertainties of the T-type thermocouples, pressure transducers, dimensions, the variable transformer, and the resistive heaters were $\pm 0.5℃$, 0.25% of the full scale, $\pm 2.54 \times 10^{-2}$ mm, $\pm 2\%$ of the voltage, and $\pm 5\%$ of the electrical resistance, respectively. The uncertainty of the property R that is a function of variables X_1, X_2, …, X_N, is calculated as follows [20]:

$$\delta R = \sqrt{\sum_{i=1}^{N} \left(\frac{\partial R}{\partial X_i} \delta X_i \right)^2} \tag{7}$$

where δX_i is the uncertainty of the ith measured value. The maximum uncertainties of heat flux and thermal resistance in the present study were below 7.8% and 8.4%, respectively.

III. Results

Fig. 4 compares the thermal resistances at different heat fluxes for two flow rates. A monotonic decrease in the thermal resistance by increasing the heat load at both flow rates indicates a two-phase heat transfer inside the heat sink; otherwise, a flat curve for $R - q$ was expected, which indicated a single-phase heat transfer. Increasing the heat load leads to a higher rate of boiling heat transfer, which results in a monotonic decrease in the thermal resistance. This trend continues until the partial dryout happens, which is identified when the slope of $R - q$ curve is changed. The partial dryout corresponds to an insufficient liquid over the evaporator, and accelerates the critical heat flux (CHF) and ultimately the heater failure. The continuously decreasing the thermal resistance with increasing the heat loads at the present experiments signifies that the partial dryout did not happen at any flow rates. At both flow rates, the heat sink operated up to a moderately high heat flux ~183 W/cm^2 with a measured thermal resistance of 0.32 K-cm^2/W.

A wall superheat represents the difference between the surface temperature and the saturation temperature. The boiling heat transfer starts at a sufficiently large wall superheat such that below this threshold value, the heat transfer inside the heat sink is single-phase. A high inlet subcooling degree in the present study results in a delay to reach the threshold wall superheat to initiate boiling. As a result, a single-phase convection heat transfer plays a key role in the cooling mechanism, particularly at lower heat fluxes due to a longer delay for reaching the threshold wall superheat. A slight decrease in the slope of the $R - q$ curve at the higher flow rate indicates a greater impact of single-phase convection heat transfer compared to the lower flow rate, which is expected due to a higher inlet subcooling degree at the higher flow rate. The inlet temperature was maintained almost the same at both flow rates; as a result, the single-phase heat transfer coefficient enhances by increasing the flow rate. For this reason, up to the heat flux ~ 100 W/cm^2, a lower thermal resistance is achieved at 0.51 LPM compared with the flow rate at 0.31 LPM. A sharper decrease in the slope of $R - q$ curve at lower flow rate corresponds to a an earlier starting the two-phase heat transfer inside the heat sink operating at the lower flow rate. This is expected because the inlet subcooling degree at the lower flow rate is much smaller than that of the higher flow rate. Due to a delay in starting the boiling heat transfer at the larger flow rate, a sharp decrease in the thermal resistance of the heat sink at the higher flow rate is expected beyond the maximum heat flux in the present study. This is due to the dominance of the boiling heat transfer. However, the experiments were not continued at higher heat loads to avoid very hot temperatures of the resistive heaters.

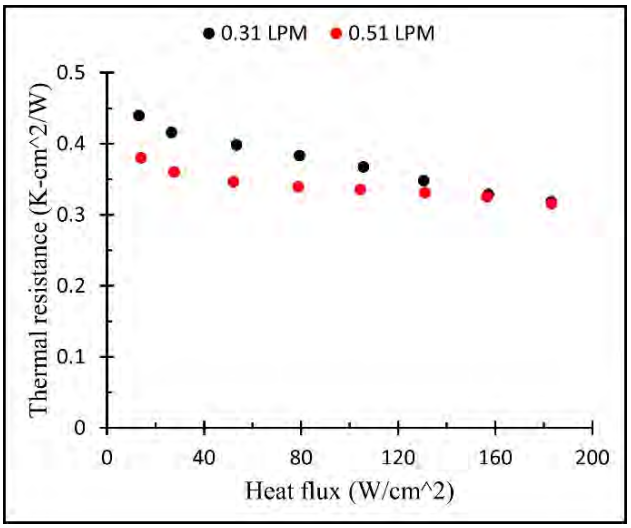

Fig. 4. Thermal resistance at different heat fluxes.

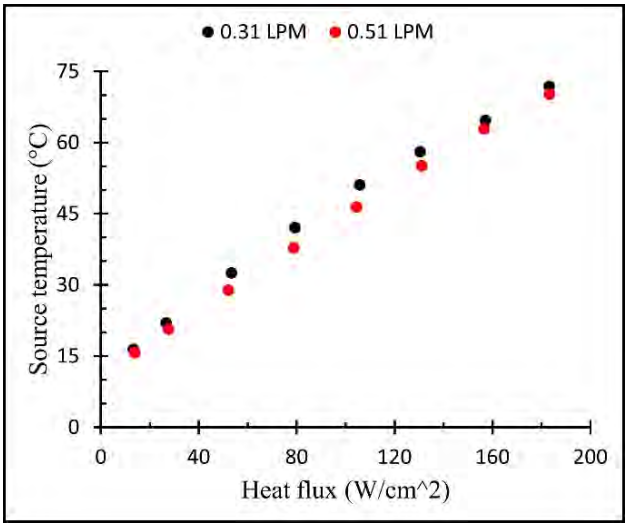

Fig. 5. Source temperature at different heat fluxes.

Fig. 5 illustrates the source temperature at different heat fluxes. At both flow rates, the maximum temperature of the heater was maintained below 75 °C.

The pumping power (P_p), calculated below, is a key design parameter such that a large P_p may impede using the cooling system regardless of its low thermal resistance [21,22]:

$$P_p = \dot{V} \times \Delta P \tag{8}$$

where $\dot{V}$ and ΔP correspond to the volume flow rate and the pressure drop across the heat sink, respectively. One of the main

significances of a pumped two-phase technology is operation with substantially lower flow rates compared with a single-phase liquid-cooled system to remove a given amount of heat. Although the generation of vapor leads to an increased ΔP in a two-phase heat sink, operation with low flow rate lowers the P_p compared with the single-phase liquid system. In the present experiments, corresponding maximum P_p at the flow rate of 0.31 LPM and 0.51 LPM was below 0.14 W and 0.54 W, respectively. The higher P_p at a higher flow rate is expected due to both higher ΔP and $\dot{V}$.

The developed heat sink in the present study as a low-CTE, dielectric, and CTE-matched TMS with operation within low pumping power is a promising efficient cooling system for direct mounting of high heat flux electronics on the heat sink.

IV. Conclusion

Highly thermal conductive and low-CTE two-phase minichannel heat sink made of AlN substrate was fabricated and tested over a wide range of heat fluxes at two different flow rates. To ensure that the heat sinks is CTE-matched for minimizing the thermal stress in the joint surfaces, the enclosure of the heat sink was made of Kovar, which has similar CTE's value with AlN. The working fluid was R245fa due to its reasonably low vapor pressure. Monotonic decrease in the thermal resistance of the heat sink by increasing heat load was achieved without any indication of partial dryout. The heat sink operated up to a heat flux ~ 183 W/cm^2 with a thermal resistance of 0.32 K-cm^2/W. The combination of high thermal conductivity of AlN, its low CTE, and low dielectric constant along with its CTE-matched with Kovar make AlN-Kovar heat sink a promising TMS for high-heat-density electronic applications. The copper layer on the DBC AlN substrate allows sintering copper powders on the substrate, which enhances boiling heat transfer. Future work will involve wicked heat sink that is expected to substantially reduce the thermal resistance due to thin film evaporation in the wick. Also, the capillary forces generated by wick can substantially enhance the CHF. As a result, wicked heat sinks made of DBC AlN substrates will potentially allow an increase in the power of future electronic devices beyond the current state-of-the-art.

Acknowledgment

Support by the Office of Science in the U.S. Department of Energy, award number DE-SC0018845 is acknowledged.

References

[1] Ryelandt S, Mertens A and Delannay F 2015 Al/stainless-invar composites with tailored anisotropy for thermal management in light weight electronic packaging *Mater. Des.* **85** 318–23

[2] Adera S, Antao D, Raj R and Wang E N 2016 Design of micropillar wicks for thin-film evaporation *Int. J. Heat Mass Transf.* **101** 280–94

[3] Drummond K P, Back D, Sinanis M D, Janes D B, Peroulis D, Weibel J A and Garimella S V 2018 A hierarchical manifold microchannel heat sink array for high-heat-flux two-phase cooling of electronics *Int. J. Heat Mass Transf.* **117** 319–30

[4] Kim S-M and Mudawar I 2013 Universal approach to predicting saturated flow boiling heat transfer in mini/micro-channels – Part II. Two-phase heat transfer coefficient *Int. J. Heat Mass Transf.* **64** 1239–56

[5] Shaeri M R, Attinger D and Bonner R W 2018 Vapor chambers with hydrophobic and biphilic evaporators in moderate to high heat flux applications *Appl. Therm. Eng.* **130** 83–92

[6] Nie Q, Chen G, Wang B, Yang L and Tang W 2021 Process optimization, microstructures and mechanical/thermal properties of Cu/Invar bi-metal matrix composites fabricated by spark plasma sintering *Trans. Nonferrous Met. Soc. China* **31** 3050–62

[7] Chen H, Zheng F, Cheng W, Tao P, Song C, Shang W, Fu B and Deng T 2021 Low thermal expansion metal composite-based heat spreader for high temperature thermal management *Mater. Des.* **208** 109897

[8] Otiaba K C, Ekere N N, Amalu E H, Bhatti R S and Mallik S 2011 Thermal Management Materials for Electronic Control Unit: Trends, Processing Technology and R and D Challenges *Adv. Mater. Res.* **367** 301–7

[9] Zhou C, Ji G, Chen Z, Wang M, Addad A, Schryvers D and Wang H 2014 Fabrication, interface characterization and modeling of oriented graphite flakes/Si/Al composites for thermal management applications *Mater. Des.* **63** 719–28

[10] Kelly A 2007 Composite Materials for Thermal Expansivity Matching and High Heat Flux Thermal Management *Key Eng. Mater.* **334–335** 1017–20

[11] Savrun E 2002 Packaging considerations for very high temperature microsystems *Proceedings of IEEE Sensors* IEEE SENSORS 2002 vol 2 (Orlando, FL, USA: IEEE) pp 1139–43

[12] Shenogin S, Ferguson J, Ganguli S and Roy A K 2021 Studying the applicability of amorphous metal alloys as interface material for power electronics packaging *Materialia* **18** 101142

[13] Chen C, Xue Y, Li X, Wen Y, Liu J, Xue Z, Shi D, Zhou X, Xie X and Mai Y-W 2019 High-performance epoxy/binary spherical alumina composite as underfill material for electronic packaging *Compos. Part Appl. Sci. Manuf.* **118** 67–74

[14] Dussinger P, Ju Y S, Catton I and Kaviany M 2012 High heat flux, high power, low resistance, low CTE two-phase thermal ground planes for direct die attach applications *Ann Arbor* **1001** 48109

[15] Yu C, Buttay C and Laboure E 2017 Thermal Management and Electromagnetic Analysis for GaN Devices Packaging on DBC Substrate *IEEE Trans. Power Electron.* **32** 906–10

[16] Kandlikar S G and Balasubramanian P 2004 An Extension of the Flow Boiling Correlation to Transition, Laminar, and Deep Laminar Flows in Minichannels and Microchannels *Heat Transf. Eng.* **25** 86–93

[17] Ju Y S, Kaviany M, Nam Y, Sharratt S, Hwang G S, Catton I, Fleming E and Dussinger P 2013 Planar vapor chamber with hybrid evaporator wicks for the thermal management of high-heat-flux and high-power optoelectronic devices *Int. J. Heat Mass Transf.* **60** 163–9

[18] Lee J and Mudawar I 2009 Critical heat flux for subcooled flow boiling in micro-channel heat sinks *Int. J. Heat Mass Transf.* **52** 3341–52

[19] Shaeri M R, Bonner R W and Ellis M C 2020 Thin hybrid capillary two-phase cooling system *Int. Commun. Heat Mass Transf.* **112** 104490

[20] Shaeri M R, Attinger D and Bonner R 2017 Feasibility study of a vapor chamber with a hydrophobic evaporator substrate in high heat flux applications *Int. Commun. Heat Mass Transf.* **86** 199–205

[21] Botchway K-D and Shaeri M R 2022 The Effect of Locations of Inlet and Outlet Manifolds on Thermal Performance of a Lithium-Ion Battery Thermal Management System The 7th World Congress on Momentum, Heat and Mass Transfer

[22] Shaeri M R and Bonner R W 2018 Lightweight and high-performance air-cooled heat sinks *2018 34th Thermal Measurement, Modeling & Management Symposium (SEMI-THERM)* 2018 34th Thermal Measurement, Modeling & Management Symposium (SEMI-THERM) (San Jose, CA: IEEE) pp 224–7